Identification of cracks in shafts using magnetic bearings

Cesar Augusto Fonseca[1], Michael Kreutz[2], and Thomas Thümmel[2]

[1] Post-Graduation Center of the Brazilian Navy, CIAW,
Rio de Janeiro, Brazil
cesar.linhares@marinha.mil.br
[2] Dept. of Mechanical Eng., Technische Universität München (TUM),
Garching bei München, Germany
m.kreutz@tum.de, th.th.thuemmel@gmail.com

Abstract

This paper shows an experimental approach to the identification of cracks on magnetically levitated rotors. The crack is artificially done to shaft in such a way that the breathing crack model is no longer representative and the responses are compared against the normal shaft operating in the same conditions. The experiments have been conducted the shaft rotates at 400 RPM, away from any natural frequency, and the influence of this severe crack was assessed using white noise excitation added to the control signal of one of the magnetic bearings. It has been observed shifts on the higher resonances when rotor is either rotating or not of around 10 Hz lower for the damaged rotor. A Finite Element Model is proposed and, using the same identified parameters of the test rig, it reproduced the same changes in the frequency domain.

Keywords: Crack detection, Magnetic Bearing, Modal Analysis

1 Introduction

Magnetically levitated rotors have become more common in recent years, due to its frictionless features and the capacity to achieve high angular velocities, causing cost reduction in maintenance and efficiency. They are found in centrifuges, vacuum pumps, flywheels, and compressors.

Normally, the behavior a rotor on an ordinary bearing is well known, but the demand for higher angular velocities and lower to none friction power loss makes the magnetic bearing a powerful solution [1]. The downside is that the low damping may not be able to contain occasional instabilities and the rotor is constantly dependent on the power supply for the active control system [2]. In the event of power loss or a complete failure of the monitoring system, a magnetic bearing requires mechanical protection such as safety bearings to support a possible rotor drop [3].

The most common type of failure found in rotatory systems is the unbalance, which increases the lateral vibration causing the excessive forces in the bearings [4]. Other eventualities can happen at electrical and control systems, with problems regarding the sensors and/or actuators [5, 6]. Therefore, magnetically levitated rotors are endowed with a monitoring system that is constantly checking potential signs of damage or any kind of problems.

The monitoring system is active while the rotor is running and the faster the rotor spins, the more precise it has to be to perform a diagnosis of the machine. Each type of damage can create a clue or a signal that, compared to a model-based program, is easily identified. In the work of Roßner [7] many types of failures on a rotor are addressed such as unbalance, axle curvature and roundness failure of the shaft. Guangming and Jin [8] approach the same problem on a still standing rotor using a finite element model.

The detection of failures of rotors through the use magnetic bearings has been addressed by [9, 10, 11] and other published papers studied the effects of crack on the dynamics of a

rotor for identification and diagnosis [12, 13, 14, 15]. The cracks are usually represented by the "breathing crack" model, see ref. [16], as it opens and closes following the bending of the shaft as it is turning. These models are extensively studied over the last years.

The present work describes a study conducted experimentally on a fully monitored rotor with two magnetic bearings, whose shaft has a crack close to its middle point. The rotor was excited by white noise on one of the magnetic bearings and displacement and force signals are captured on other sections of the shaft. The response is compared to an undamaged rotor upon the same conditions. Then, a finite element model is created to reproduce the overall behavior of the test rig. Unlike previous works, the crack is too wide to closes itself while the rotor is turning, so the effects of the crack on the shaft are investigated through a shift of higher natural frequencies on the frequency response functions and time evolution of orbit plots, either experimentally or numerically.

2 The test bench

The test bench is shown in Figure 2a and its components in Figure 2b. The machine is constituted of a rotor, which is levitated by two magnetic bearings close to its extremities, an 8mm diameter/700mm long shaft. It is powered by a servo motor on a Cardan joint and on the other end is free. The servo motor is controlled by a real time system dSPACE board which also serves to gather data from the set of sensors assembled to the test rig and emits to and received data from a Matlab/Simulink program. Inside the magnetic bearing there is a mechanical gap between the rotor and the backup bearing which is comprised of 1.4mm and 2.5mm at the disk. The whole system is levitated by active magnetic bearings and the lateral displacement is captured at the bearings and at the disk by eddy current sensors. The sensors are mounted in a way that the coordinates x and y are orthogonally measured and their middle values are given as set point of the PID-Controller for the magnetic bearings to adjust the electrical current of the magnetic coils. The position at the disk is measured by laser sensors and the angular velocity by an encoder close the joint. Additionally to the controller forces, an excitation signal is provided by the magnetic bearings to serve as input force for the conditioning monitoring system see Figure 1. It is a burst random noise applied by the magnetic bearing on the right near the extremity. Besides, the force components applied by the magnets are also measured since the bearing is mounted on a force transducers. For further details of the test rig construction are available in [19].

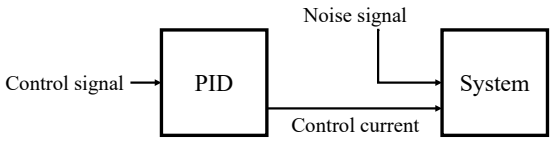

Figure 1: Added noise to the magnetic bearing current control.

Since the displacements and the input forces are assessed, then it is possible to perform an Experimental Modal Analysis (EMA) of the rotor, either if it is rotating or at standstill. Previous analysis of the rotor had been performed by [18, 19] comparing the experimental results with a Finite Element Model (FEM). The Frequency Response Function of the rotor is determined in two conditions; when it is rotating at 400 RPM and at standstill, 0 RPM. Now, another shaft with the same characteristic is deliberately sawn to create a defect, see Figure 3.

A 3mm deep and 1 mm wide crack is created on the shaft close to the middle point of the shaft near the disk. The damaged rotor replaces the healthier one and the experiment is run with the conditions and the added white noise.

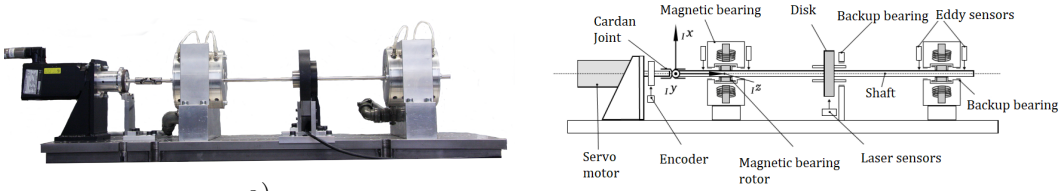

Figure 2: a) Photo of the test bench. b) Rotor scheme. Adapted from [18] and [19].

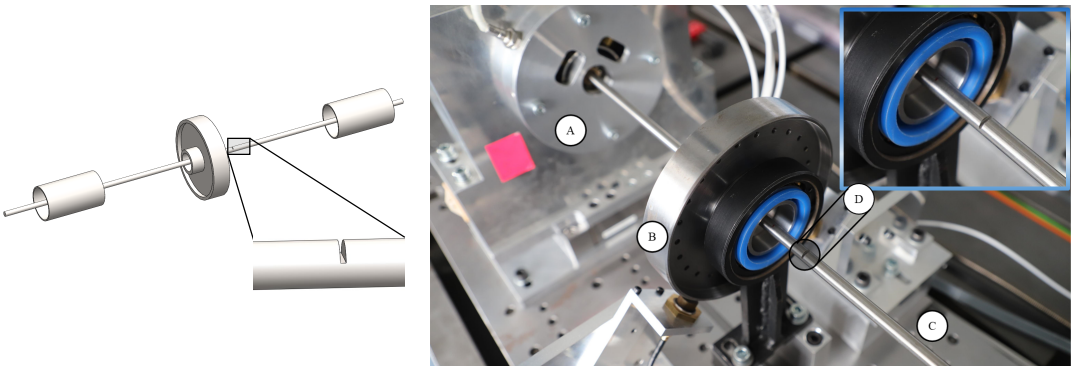

Figure 3: Left: CAD drawing with detail of the crack on the shaft. Right: Detail of the test rig. A - Magnetic Bearing; B - Disk; C - Shaft; D - Crack on the shaft.

3 Experimental run-up and results

The rotor is set to spin at an angular velocity of 400 RPM $\approx$ 6.66 Hz for 600 seconds and the signals from the displacements at the bearings and the disk and the forces are acquired. The orbit plots at position 67.5 mm from the coupling is shown in Figure 4 after the transient attenuates. A smoothed line is drawn to mitigate the noisy raw data. Additionally, one may notice that inner loops orbits related to the breathing crack cases do not appear.

The Frequency Response Functions (FRF) of the lateral displacement at position 630 mm is calculated and plotted to investigate variations of the natural frequencies on the presence of the crack. In Figure 5a and b one can see the FRFs of the normal rotor and the damaged rotor respectively. In both figures, the red plot is the standstill case and the blue the rotating case. The FRF spans up to 250 Hz, because above this threshold the coherence falls sharply to zero, due to the limited bandwidth of the excitation signal till this frequency.

The experiments show that the vibration of the rotor increased considerably due to the existing serious damage. The FRFs of the rotor of the lateral displacement show that there is a shift of some resonances around 110Hz, 160 Hz, and 210 Hz, but some remain practically the same.

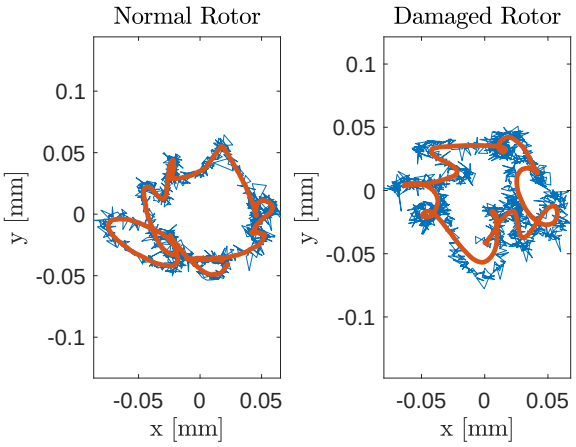

Figure 4: Experimental orbit plots.

At standstill, the angular position of the crack showed almost no influence compared to the normal shaft, but as the shaft rotates, then it is possible to see changes on the spectra. The main difference between the normal shaft and the damaged shaft is observed at the resonance at 210 Hz. The peak decreases considerably and it moves clearly to the left.

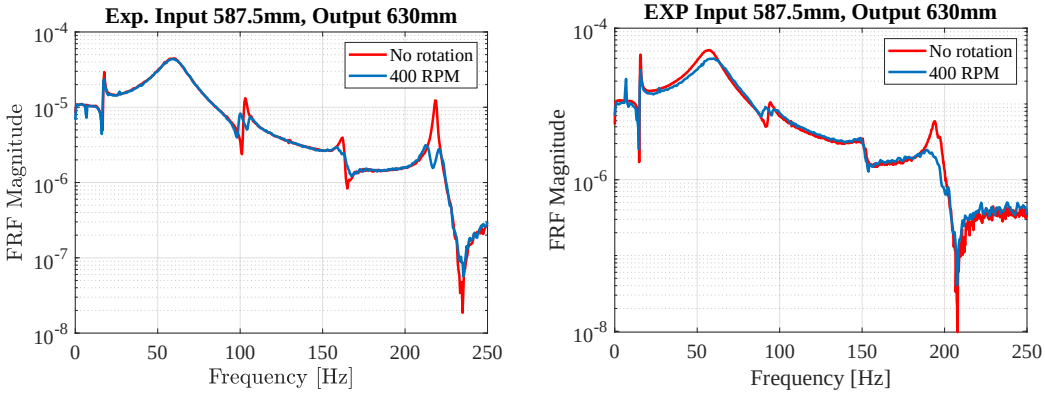

Figure 5: FRF of both rotors. a) Normal shaft. b) Damaged shaft.

4 Mathematical Model

The Finite Element Method (FEM) is implemented in order to achieve a representative numerical model for the rotor-bearing lateral vibration. The equations of motion are defined as:

$$M\ddot{X} + (D - G(\Omega))\dot{X} + KX = f(t), \tag{1}$$

where M is the global mass matrix, D is the damping matrix and K is the stiffness matrix. Each element has two nodes with four degrees of freedom, two linear and two angular displacements, and all of them are represented by the vector X. The mass matrices of shaft elements due to linear and angular movements are given as

$$M_e^T = \frac{\rho A l}{420}\begin{bmatrix} 156 & 0 & 0 & 22l & 54 & 0 & 0 & -13l \\ 0 & 156 & -22l & 0 & 0 & 54 & 13l & 0 \\ 0 & -22l & 4l^2 & 0 & 0 & -13l & -3l^2 & 0 \\ 22l & 0 & 0 & 4l^2 & 13l & 0 & 0 & -3l^2 \\ 54 & 0 & 0 & 13l & 156 & 0 & 0 & -22l \\ 0 & 54 & -13l & 0 & 0 & 156 & 22l & 0 \\ 0 & 13l & -3l^2 & 0 & 0 & 22l & 4l^2 & 0 \\ -13l & 0 & 0 & -3l^2 & -22l & 0 & 0 & 4l^2 \end{bmatrix}, \tag{2}$$

$$M_e^R = \frac{\rho A r^2}{120 l}\begin{bmatrix} 36 & 0 & 0 & 3l & -36 & 0 & 0 & 3l \\ 0 & 36 & -3l & 0 & 0 & -36 & -3l & 0 \\ 0 & -3l & 4l^2 & 0 & 0 & 3l & -l^2 & 0 \\ 3l & 0 & 0 & 4l^2 & -3l & 0 & 0 & -l^2 \\ -36 & 0 & 0 & -3l & 36 & 0 & 0 & -3l \\ 0 & -36 & 3l & 0 & 0 & 36 & 3l & 0 \\ 0 & -3l & -l^2 & 0 & 0 & 3l & 4l^2 & 0 \\ 3l & 0 & 0 & -l^2 & -3l & 0 & 0 & 4l^2 \end{bmatrix}, \tag{3}$$

where the global mass matrix $M = M_e^T + M_e^R$. The gyroscopic and stiffness matrices of the shaft elements due to bending are presented respectively as follows:

$$G_e = 2\Omega\frac{\rho A r^2}{120 l}\begin{bmatrix} 0 & -36 & 3l & 0 & 0 & 36 & 3l & 0 \\ 36 & 0 & 0 & 3l & -36 & 0 & 0 & 3l \\ -3l & 0 & 0 & -4l^2 & 3l & 0 & 0 & l^2 \\ 0 & -3l & 4l^2 & 0 & 0 & 3l & -l^2 & 0 \\ 0 & 36 & -3l & 0 & 0 & -36 & -3l & 0 \\ -36 & 0 & 0 & -3l & 36 & 0 & 0 & -3l \\ -3l & 0 & 0 & l^2 & 3l & 0 & 0 & -4l^2 \\ 0 & -3l & -l^2 & 0 & 0 & 3l & 4l^2 & 0 \end{bmatrix}, \tag{4}$$

$$K_e = \frac{EI}{l^3}\begin{bmatrix} 12 & 0 & 0 & 6l & -12 & 0 & 0 & 6l \\ 0 & 12 & -6l & 0 & 0 & -12 & -6l & 0 \\ 0 & -6l & 4l^2 & 0 & 0 & 6l & 2l^2 & 0 \\ 6l & 0 & 0 & 4l^2 & -6l & 0 & 0 & 2l^2 \\ -12 & 0 & 0 & -6l & 12 & 0 & 0 & -6l \\ 0 & -12 & 6l & 0 & 0 & 12 & 6l & 0 \\ 0 & -6l & 2l^2 & 0 & 0 & 6l & 4l^2 & 0 \\ 6l & 0 & 0 & 2l^2 & -6l & 0 & 0 & 4l^2 \end{bmatrix}. \tag{5}$$

The parameters ρ, E, I, A and r stand for the linear density, the Young modulus for steel, the area moment of inertia, the cross section area, and the radius of the shaft, respectively. The term l is the length of the element. The shaft is divided into elements of 1cm each, except for the region near the crack where the length reduces to 1mm. Smaller sizes of the elements did not increased the accuracy analytical results, see ref. [18]. Since the magnetic bearing aligns the center of the shaft and it develops small displacements, the magnetic force is considered linear with a constant spring coefficient and a damping term:

$$F_{\text{mag}} = k_{\text{mag}} X|_{\text{bearing}} + d_{\text{mag}} \dot{X}|_{\text{bearing}}. \tag{6}$$

These coefficients are inserted into the specific node of the magnetic bearing. The properties of the disk and the bearings are considered punctual and are added on their corresponding nodes. The elements affected by these components have their radii increased by 0.8mm to reproduce the stiffening caused by the connection between the components and the shaft.

The global damping matrix follows the Rayleigh model $D = \alpha M + \beta K$. The determination of α and β comes from the experimental data, which resulted in $\alpha = 0$ and $\beta = 10^{-5}$.

To determine the rotor's frequency response function analytically, one has to analyze the transfer function of equation (1) in the frequency domain as:

$$H(\omega) = \left| \left[(2\pi i\omega)^2 M + (D - G(\Omega)) 2\pi i\omega + K \right]^{-1} \right|. \tag{7}$$

4.1 The crack in the Finite Element Model

The usual representation of cracks in rotors is the breathing model in which the crack exhibits a dynamics of its own, as the rotor executes a full rotation. The crack is completely open when it is positioned downwards and closes when upwards. This is usually modeled by time-varying stiffness terms. In the present work, the crack does not close itself, due to its width and depth. Thus, the damage is described by removing the mass and gyroscopic terms on the cracked node from the mass and gyroscopic matrices. The element's stiffness is affected by taking the moment of inertia of the remaining element piece. Therefore, the effect is no longer represented as time varying.

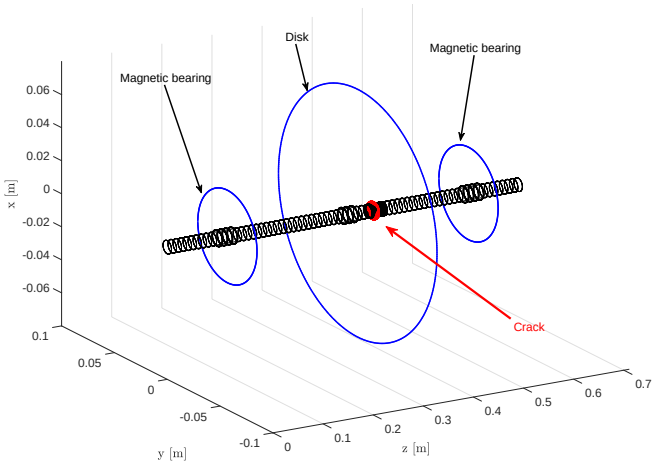

Figure 6: FEM mesh of the rotor.

The proposal of the model is backed up by the experimental data. In Figure 7, one can see the FFT of the lateral vibration of the normal and damaged rotors. The breathing crack case would exhibit peaks at $\Omega/2$ and $\Omega/3$, which do not appear in the frequency domain.

4.2 Numerical analysis

The shaft's parameters shown in Table 1 are used to assemble the matrices necessary for equation (1). Then, Table 2 summarizes the features of the finite element mesh, in which the nodal positions of the crack, disk and bearings are presented.

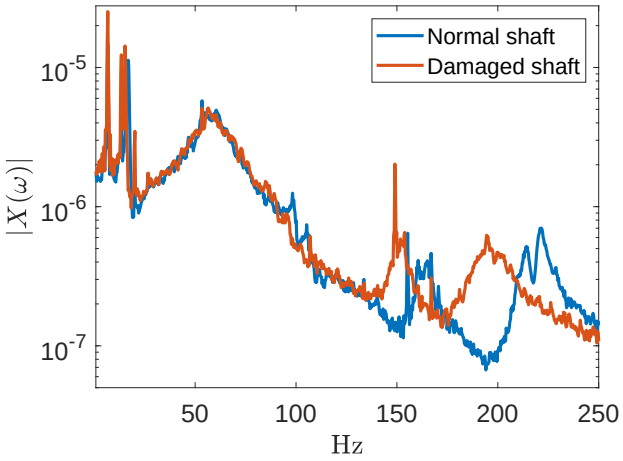

Figure 7: Experimental FFT of the lateral displacement of the rotor. $\Omega = 400$ RPM.

Table 1: Physical parameters of the rotor.

Parameter	Value
ρ	7860 kg/m^3
E	2.11×10^{11} Pa
A	5.0265×10^{-5} m^2
I	2.01×10^{-10} m^4
r	4×10^{-3} m
k_{mag}	1.1×10^{5} N/m
d_{mag}	20 Ns/m
Ω	400 RPM
I_{crack}	1×10^{-11} m^4
A_{crack}	33×10^{-6} m^2
M_{disk}	2276 g
$I_{\text{disk},x,y}$	1.5×10^{-3} kg$\cdot$ m^2
$I_{\text{disk},r}$	2.8×10^{-3} kg$\cdot$ m^2
M_{bearing}	851 g
$I_{\text{bearing},x,y}$	4.84×10^{-4} kg$\cdot$ m^2
$I_{\text{bearing},r}$	4.03×10^{-4} kg$\cdot$ m^2

Figures 8 illustrates the modal analysis of the rotor for two scenarios, one whose angular velocity is zero and the second one in which it is 400 RPM. The FEM shows a shift of the higher natural frequencies, which follows the same trend as the one captured experimentally as may be seen in Figure 5. For the standstill case, the natural frequency around the 210 Hz reduces to 200 Hz. Likewise, the lower natural frequency of 110 Hz decreases slightly, but the one in the middle does not shift as it does for the experimental set up. Similarly, it can be seen in Figure 8, *i.e.* $\Omega = 400$ RPM, that the peaks are lower in the case of the damaged shaft.

A time integration of equation (1) is performed using a Newmark algorithm, [20]. The force vector $f(t)$ includes an unbalance force located at the position of the disk and whose magnitude

Table 2: Mesh features of both normal and damaged shaft.

		Normal	Damaged
# Elements		70	97
DoF		284	397
crack	node	-	51
	position	42 cm	
disk	node	39	39
	position	39 cm	
bearing	node	13 and 63	13 and 89
	position	12 cm and 62 cm	
maximum element length		1 cm	1 cm
minimum element length		1 cm	1 mm

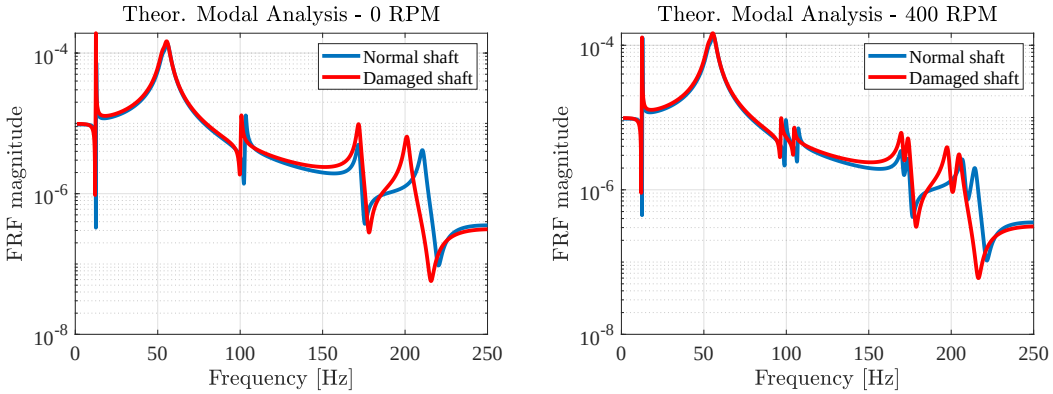

Figure 8: FEM modal analysis. a) Zero angular velocity. b) 400 RPM angular velocity.

is $U = 2.805 \times 10^{-4}$ kg·m. The time integration iterates every 10^{-3} s and spans up to 60 s. The initial conditions for all nodal degrees of freedom are set to zero except for the last linear velocity at the free tip of the shaft, which begins with 1.0 m/s. Besides, the rotor is has the same angular velocity of 400 RPM.

The orbit plots from the normal shaft and the damaged one are shown in Figures 9a and 9b. The transient is clearly seen as the rotor slowly settles into a circular trajectory, Figure 9c. As expected, the damaged rotor executes a larger orbit.

5 Conclusion

The present work investigated the effects caused by a deep and wide crack upon the dynamics of a rotor supported by magnetic bearings. These cracks do not follow the conventional breathing crack model as it stays open during the whole rotation of the shaft. The experiments showed that overall the natural frequencies were affected by the damage, which were observed to be found at least 10 Hz lower than the healthier shaft. A finite element model was employed to reproduce the phenomena and could approximate the FRF numerically with the one calculate with experimental data.

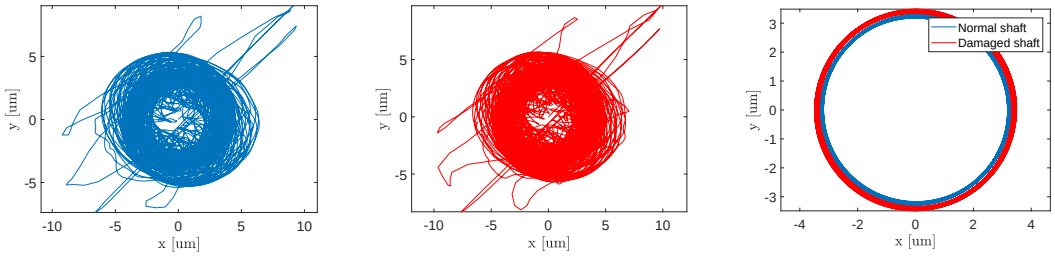

a) b) c)

Figure 9: Orbit plots of the two scenarios at 400 RPM. a) the normal shaft. b) the damaged shaft. c) Orbits after the transient is damped.

The model is by and large a linear approach to the problem in question, but it eventually manages to reproduce the phenomena. Also, this set up indicates the possibility of using magnetic bearings to identify a problem without stopping the machine by adding a noise as an additional excitation to the control signal. Further improvement can be done to the model, by taking into account that the location of the crack creates an asymmetric rotor and nonlinearities of the magnetic forces. Besides, the coupling between the driving motor and the shaft is not considered, which indeed does influence the dynamics of the system.

References

[1] Maslen E.H., Schweitzer G., (2009) Magnetic bearings. Springer, Heidelberg. https://doi.org/10.1007/978-3-642-00497-1

[2] Schweitzer, G. *Applications and Research Topics for Active Magnetic Bearings*, IUTAM Symposium on Emerging Trends in Rotor Dynamics pp 263-273

[3] Fonseca, C. A., Santos, I. F., Weber, H. I. *An experimental and theoretical approach of a pinned and a conventional ball bearing for active magnetic bearings*, December 2020, Mechanical Systems and Signal Processing, 138, page 106541, DOI: 10.1016/j.ymssp.2019.106541

[4] Mogal, S.P., Lalwani, D.I.: *A brief review on fault diagnosis of rotating machineries.* Appl. Mech. Mater. 541–542, 635–640 (2014)

[5] Zhang, Y.Z., Zhang, L.Z., Luo, X.Y., Guan, X.P.: *Sensor/actuator faults detection for networked control systems via predictive control.* Int. J. Autom. Comput. 10(3), 173–180 (2013)

[6] Tsai, C., King, Y.H., Lee, R.M.: *Fault diagnosis for magnetic bearing.* Mech. Syst. Signal Process. 23(4), 1339–1351 (2009)

[7] Roßner, M. *Modellbasiertes Monitoring von Rotoren mit mehreren gleichzeitigen Fehlern.* PhD Thesis. Technische Universität München, 2015, 166 pages. ISBN: 9783843923965

[8] Guangming Dong, Jin Chen, *Vibration analysis and crack identification of a rotor with open cracks*, Japan J. Indust. Appl. Math. (2011) 28:171–182 DOI: 10.1007/s13160-011-0031-3

[9] Mani, G., Quinn, D.D., Kasarda, M.: *Active health monitoring in a rotating cracked shaft using active magnetic bearings as force actuators.* J. Sound Vib. 294, 454–465 (2006)

[10] Silva, G.M., Pederiva, R.: *Diagnosis in a rotor supported by active magnetic bearings.* In: Proceedings of the 7th IFToMM International Conference on Rotor Dynamics, International Federation for the Promotion of Mechanism and Machine Science, 2006 Vienna, Austria

[11] Thümmel, T., Rossner, M., Wagner, C., Maierhofer, J. and Rixen, D., *Rotor Orbits at Operation Speed and Model-Based Diagnosis of Multiple Errors.* In: Cavalca K., Weber H. (eds) Proceedings of

the 10th International Conference on Rotor Dynamics – IFToMM. Vol. 2 (2018). DOI: 10.1007/978-3-319-99268-6_16.

[12] Al-Shudeifat, M.A., Butcher, E.A.: *New breathing functions for the transverse breathing crack of the cracked rotor system: approach for critical and subcritical harmonic analysis*. J. Sound Vib. 330, 526–544 (2011)

[13] Cavalini Jr., A.A., Sanches, L., Bachschmid, N., Steffen Jr., V.: *Crack identification for rotating machines based on a nonlinear approach.* Mech. Syst. Signal Process. 79, 72–85 (2016)

[14] Guo, C., Yan, J., Yang, W.: *Crack detection for a Jeffcott rotor with a transverse crack: an experimental investigation.* Mech. Syst. Signal Process. 83, 260–271 (2017)

[15] Bachschmid, N., Pennacchi, P., Tanzi, E.: *A sensitivity analysis of vibrations in cracked turbogenerator units versus crack position and depth.* Mech. Syst. Signal Process. 24, 844–859 (2010)

[16] Gasch, R.: *A survey of the dynamic behaviour of a simple rotating shaft with a transverse crack.* J. Sound Vib. 160, 313–332 (1993)

[17] Silva, G.M., Pederiva, R. *Unbalance Identification in a Rotor Supported by Active Magnetic Bearing* IFToMM 2018, pp. 82–96, (2019) DOI: 10.1007/978-3-319-99262-4_7

[18] Kreutz, M., Maierhofer, J., Thümmel, T., Rixen, D., 2020. *Modaler Modellabgleich eines Rotors in Magnetlagern.* Sechste IFToMM D-A-CH Konferenz 2020. DOI: 10.17185/duepublico/71192

[19] Maierhofer, J., Thümmel, T., Rixen, D., *Modellbasiertes Monitoring an magnetgelagerten Rotoren.* In: SIRM 2017 (2017), S. 1–10

[20] Cunha, A., Soize, C. & Sampaio, R. Computational modeling of the nonlinear stochastic dynamics of horizontal drillstrings. Comput Mech 56, 849–878 (2015). DOI: 10.1007/s00466-015-1206-6